



Metal flowing mechanism of high-speed cold roll beating of spline

Bo Qu^{1,2} · Heyong Han¹ · Zhiqi Liu¹ · Zhanlong Li¹

Received: 20 April 2021 / Accepted: 16 October 2021 / Published online: 21 January 2022
© The Author(s), under exclusive licence to Springer-Verlag London Ltd., part of Springer Nature 2021

Abstract

It is significant to master the metal flowing mechanism of high-speed cold roll beating (HSCRB) for forming quality control. The involute spline was formed at room temperature, the stress distribution and metal flowing displacement of the parts were analyzed by simulation, and the microstructure and hardness of the parts were studied by experiment. The results show that the stress at the groove is the largest and transmitted to the surrounding, and the bottom land, tooth side, and top land decrease successively. The metal flows away from the roller and the center of the workpiece, and the displacement of the bottom land, tooth side, and top land decreases successively. After multiple beats, the final tooth shape is obtained by the accumulation of flow. The metal flow results in large amount of fibrous tissue at the bottom land, a small amount of fibrous tissue at the tooth side, and no fibrous tissue at the top land. The flow results in work hardening, and the hardness is that the bottom land, tooth side, top land decrease successively, and the hardness decrease successively from the surface to the inside, showing the characteristics of hard surface and core toughness. The metal flowing mechanism was obtained. The metal in the area occupied by the roller flows in the direction of less resistance. The larger the distance to the contact area, the smaller the flow displacement. The displacement of metal flow is positively correlated with the deformation degree of microstructure and the capacity of work hardening.

Keywords High-speed cold roll beating · Metal flow · Work hardening · Forming · Microstructure

1 Introduction

High-speed cold roll beating (HSCRB) forming is a kind of advanced plastic forming which is suitable for forming splines, gears, and other tooth shaft parts at room temperature. Due to the advantages relative to the traditional machining of high efficiency, less material waste, saving energy, higher strength, and so on, the parts formed by HSCRB meet the requirement of high-demand industries, such as aerospace, wind power, nuclear power, and automobile [1].

HSCRB was proposed by Grob and Krapfenbauer [2]. Cui et al. [3] studied the residual stress of the forming parts and found that the distribution of residual stress is that the bottom land, tooth side, and top land decrease successively and the process parameters would affect the residual stress. Li

et al. [4] got external tooth grooves by HSCRB and studied the influence of process parameters on forming force and forming accuracy and found that increasing beating density and reducing spindle speed could be beneficial to forming accuracy. Niu et al. [5] studied the influence of beat on adjacent groove during the forming and found that stress wave would affect adjacent groove, but the influence is little. Tian et al. [6] proposed to use restraining device to improve the rigidity of the spline shaft and improve the forming quality by studying the vibration problem of the spline shaft during the forming.

Controlling the metal flow is beneficial to improve the forming quality [7] and prolong the life of the die [8]. The dynamic recrystallization and metal flow behavior of staggered extrusion AZ31 magnesium alloy bending products were studied, and it was found that the asymmetrical distribution of flow velocity field is one of the factors affecting the bending properties of the bending products [9]. Shen et al. [10] proposed an axisymmetric modeling to predict the metal flow in radial direction and found that the metal in the rim flowed towards the web and the metal near the surfaces of the conjunction region between the web and rim suffered

✉ Heyong Han
wjhy123@126.com

¹ School of Mechanical Engineering, Taiyuan University of Science and Technology, Taiyuan 030024, Shanxi, China

² Taiyuan Railway Machinery School, Taiyuan 030006, Shanxi, China

severe shear deformation. The characteristics of metal flow of electromechanical and hydraulic chattering were studied in the extrusion process, and it was found that with electrohydraulic chattering, the flow velocity increased, and the deformation resistance decreased, so that the method results in easy metal flow [11]. Svirin et al. [12] found that the friction coefficient has little influence on metal flow rate and the decisive factors of metal flow are plate thickness and friction coefficient. The flow velocity and pressure distribution of hollow aluminum in different directions at the extrusion outlet were analyzed to optimize the die structure and improve the concave problem [13]. Zhao et al. [14] studied the influence mechanism of metal transverse flow on the distribution of residual stress in hot rolling of strip steel and found that the preferential metal flow direction is helpful to reduce the maximum residual compressive stress, so the risk of buckling deformation reduced. Therefore, metal streamline, mesh deformation, stress field, and so on are useful methods to study metal flow. Improving metal flow conditions, such as friction conditions control [15] and process control [16], is beneficial to forming quality.

In addition, study on microstructure and mechanical properties is indispensable for plastic deformation [17, 18]. It is of great value to study the changes of microstructure and properties by severe plastic deformation [19, 20].

For the forming process, research up to date on the metal flow of the complete tooth shape of spline is insufficient. In this paper, the metal flow of the process was analyzed by tracing nodal displacement. The rule of the metal flow, the hardness, and the microstructure of the deformed spline tooth was revealed. In the research, a spline was taken as the research object, and the stress distribution and metal flow along the tooth were analyzed by finite element analysis (FEA). Experimental testing of microstructure and hardness of the tooth and the change of microstructure and hardness show the metal flowing situation and the change of properties. By combining FEA and experiments, the relationship between stress distribution and metal flow was obtained. The characteristics of metal flow and its effect on microstructure were obtained by analyzing the displacement and the change of microstructure of metal flow. Through the analysis of metal flow and hardness, the effect of metal flow on the properties of forming parts was obtained. Based on the research, the mechanism of metal flow was obtained.

2 Finite element analysis (FEA)

The principle of HSCRB is shown in Fig. 1. At room temperature, a pair of rollers rotate around their respective rotation centers at the same speed and in the opposite direction. The rollers rotate one circle; the workpiece undergoes one beating. At the same time, the workpiece feeds so that

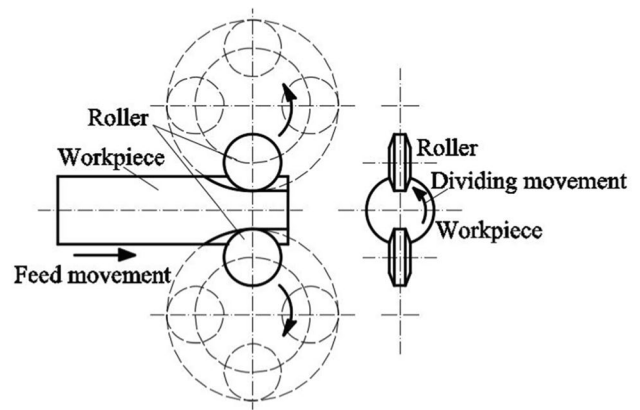


Fig. 1 The principle of HSCRB [5]

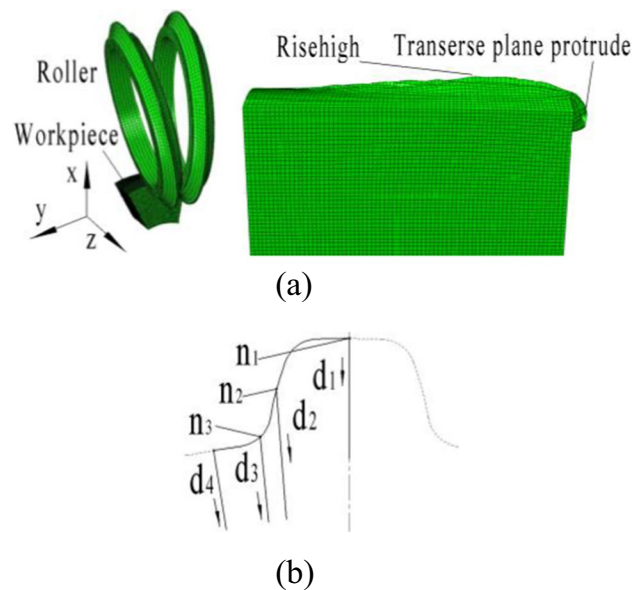


Fig. 2 Finite element simulation. **a** FEA model. **b** Nodes selection

the rollers would beat the required length of groove. The workpiece makes dividing movement when not beaten so that the rollers would beat other grooves [5]. When the rollers beat the workpiece, the workpiece undergoes plastic deformation, and the plastic deformation is the metal flow at the microscopic level. During the forming, the microstructure changed, the plastic deformation resistance of grain increases, and the plasticity and toughness decrease, resulting in work hardening. Macroscopically, the mechanical properties of the forming part changed.

FEA of the forming process was performed by ABAQUS software. On this basis, the von Mises and the metal flow were obtained. In order to improve efficiency, only two grooves were formed by two rollers to get a complete spline tooth. The FEA model is shown in Fig. 2a, and the spline

parameters are shown in Table 1. The material of the workpiece is ASTM 1045. The density, Young’s modulus, and the Poisson ratio of the material are 7890 kg/m³, 209 GPa, and 0.269, respectively. The mesh type of workpiece is C3D8R, and the number of elements is 155100. ALE adaptive meshing is used in the FEA. The beating roller is a discrete rigid body, and the friction coefficient is 0.12. The constitutive model of workpiece is Johnson–Cook (J-C) model [21, 22]. The J-C constitutive equation is shown in Eq. (1):

$$\sigma = (A + B\epsilon^n)(1 + C\ln\epsilon^*)[1 - T^{*m}] \tag{1}$$

where σ is the equivalent yield strength; A is the yield limit; B is the hardening modulus; n is the hardening coefficient; ϵ is the equivalent plastic strain; C is the strain rate constant; ϵ^* is the dimensionless plastic strain rate; $\epsilon^* = \epsilon' / \epsilon'_0$; ϵ' is the equivalent plastic strain rate; ϵ'_0 is the strain rate reference; T^* is the homologous temperature; and m is the thermal softening coefficient.

Due to the intermittent forming process and the short contact time, the heat generated by deformation can be dissipated easy, so that the effect of temperature generated by the process can be neglected [4]. Equation (2) can be obtained as follows:

$$\sigma = (A + B\epsilon^n)(1 + C\ln\epsilon^*) \tag{2}$$

The parameters of the J–C model of the material were obtained by experiments, and A , B , n , C , m , and ϵ'_0 are 507 MPa, 320 MPa, 0.28, 0.064, 1.06, and 1 s⁻¹, respectively [23].

The rollers rotate along the y -axis and feeds along the z -axis at the same time to improve the efficiency. Others’ freedom was constrained.

The metal flow was obtained by tracking the nodal displacement. As shown in Fig. 2b, the nodes are selected to obtain the displacement.

Table 1 Spline parameters

Condition	Description
Modulus (m/mm)	2.5
Number of teeth (z)	28
Pressure angle on pitch circle of roller (\circ)	30
Rotational speed of roller $n(r/min)$	1400
Speed of feed $a/(mm/s)$	1.5

3 Experiment methods

3.1 The experiments of microstructure and hardness

As shown in Fig. 3a, a quenched and tempered ASTM 1045 steel with 0.430% C, 0.290% Si, 0.630% Mn, 0.019% P, and 0.014% S formed a spline by HSCR. The roller of HSCR is shown in Fig. 3b. The spline was cut by a wire cutting machine to get a sample. The sample was chemically corroded by 4% HNO₃ alcohol solution.

The position of top land (area 1), tooth side (area 2), bottom land (area 3), and center of the tooth (area 4) was observed by a microscope (Keyence VHX-600) to obtain the microstructure of the sample.

The hardness of the sample was measured by a HXD-1000TM micro Vickers hardness tester (Shanghai Taiming Optical Instrument Co., Ltd). The hardness test was measured along the tangent line of the addendum circle (l_1), tangent line of the reference circle (l_2), tangent line of the dedendum circle (l_3), central line of the top land (l_4), and central line of the groove (l_5). Eighteen points were measured at the tangent line of the addendum circle, each point spaced 0.2 mm apart. Twenty-eight points were measured at the tangent line of the reference circle, each point spaced 0.15 mm apart. Thirty-five points were measured at the tangent line of the dedendum circle, each point spaced 0.2 mm apart. Twenty-one points were measured at the central line of the top land, each point spaced 0.2 mm apart. Eighteen points were measured at the central line of the groove, each point spaced 0.2 mm apart.

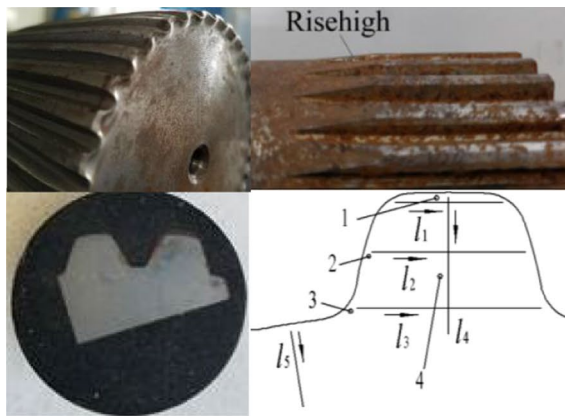
3.2 The experiment of the deformation characteristics of the groove

As shown in Fig. 3c, to supplement explanation for the deformation characteristics of the groove, the expected beat area of the pure aluminum shaft part was sliced axially to eliminate the constraints before forming a groove.

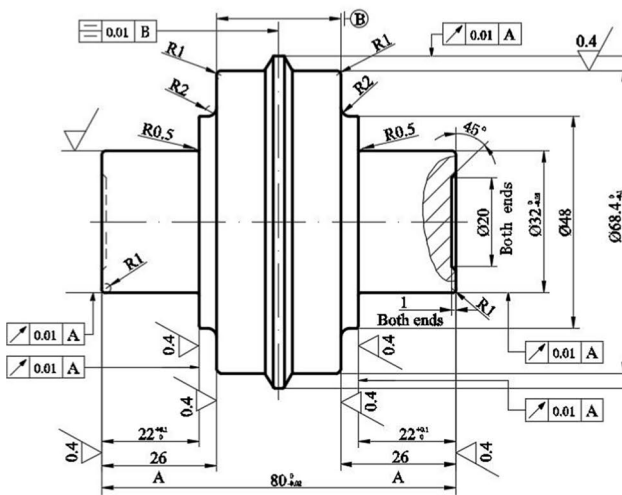
4 Results

4.1 The von Mises

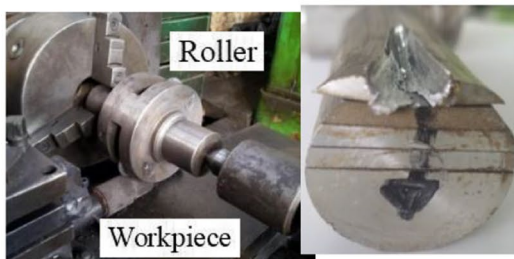
The results of von Mises can be obtained by FEA, as shown in Fig. 4; von Mises increases successively along the radial direction of top land, tooth side, and bottom land, with the maximum at the groove, which is 1301 MPa, and the minimum at the farthest end from contact area, which is 5.229 MPa. The end-to-internal tooth gradually transitions



(a)



(b)



(c)

Fig. 3 The experiments of HSCR. **a** The experiments of microstructure and hardness. **b** The roller of HSCR. **c** The experiment of the deformation characteristics of the groove

from the complete tooth profile to the original profile of the workpiece, and the groove gradually rises and finally coincides with the top land, that is, the bottom land, tooth side, and top land gradually become one, and the von Mises also gradually transitions to the same. The overall von Mises

decreases with the increase of the distance from the contact area.

4.2 Metal flow

The metal flow can be obtained by the nodal displacement. The typical nodes which are all located at the left half of the tooth were selected from FEA to get the displacement. The nodal displacement could be calculated by Eq. (3)

$$s = \sqrt{x^2 + y^2 + z^2} \quad (3)$$

where s is the nodal displacement and x , y , and z are the displacement components of the nodes on the three coordinate axes.

As shown in Fig. 2b, the first node of the 4 radial lines is located at the top land, tooth side, bottom land, and the center of the groove, respectively. The lines extend to the center of the workpiece, and each line is composed of 10 nodes (d_1, d_2, d_3, d_4). Four axial lines were selected, and the first node of each line is located at the same position as the radial line, respectively, extending the distance of 55 nodes from the end face to the interior (da_1, da_2, da_3, da_4). Three nodes of top land (n_1), tooth side (n_2), and bottom land (n_3) were selected. All nodes and lines were selected from the C cross section.

Figure 5 shows the displacement at different positions of tooth along the radial direction. Figure 6 shows the displacement at different positions along the axial direction. These figures show the metal flowing displacement after forming. As shown in Fig. 7, Fig. 8, and Fig. 9, the flowing characteristics of top land, tooth side, and bottom land during the process are reflected. One node was selected from the C cross section of each of the three positions.

As shown in Fig. 5 and Fig. 6, the metal which is under the roller is pressed to the direction of x -axis, the metal flows to the negative direction of the x -axis, and the displacement of the y -axis direction is relatively small. Adjacent metal flows in the direction of the groove due to the force of the roller, that is, the bottom land and tooth side flow in the negative direction of the x -axis, and the metal of the tooth side flows in the positive direction of the y -axis. Due to the shape of the roller, the metal which located at both sides of the roller flows away from the contact area under the extrusion by the roller, so the metal at the bottom of the tooth flows in the negative direction of the y -axis. As shown in Fig. 3c, the workpiece is processed before forming to eliminate the bottom constraint; therefore, the groove is cracked to both sides, meaning the metal flows to both sides; the result is consistent with the FEA results. The extruded metal continues to extrude the surrounding metal, which extrudes metal flow to the surface of the workpiece because of the least resistance, that is, the positive direction of the x -axis,

Fig. 4 The von Mises of FEA. **a** Top view. **b** A cross section. **c** B cross section. **d** C cross section. **e** End face. **f** The most value of von Mises

resulting in protrusions and the formation of the top land after the accumulation of many processing.

The final displacement of the top land of y-axis is relatively small, which indicates that the effect of adjacent sides of the tooth on the top land is symmetrical during forming. All nodes flow in the positive direction of the z-axis, and the displacement of the z-axis is the center of the groove, the bottom land, the tooth side, and the top land decreases successively. After forming, an arc-like protrude from the top land to the groove is formed on the end face. As shown in Fig. 6, from the end to the interior, part of the top land was not fully formed at the beginning, but after a period of forming, the top land, tooth side, and bottom land were fused together, corresponding to Fig. 3. When the tooth is fused with initial shape, the stress also tended to be the same. Compared with the end face, the interior formed is more full, owing to the sufficient material of interior and the constraints of the front end material.

The metal flowing displacement of contact area from small to large is the top land, tooth side, and bottom land. The farther from the contact area, the smaller the flow displacement. Metal flow is driven by stress; metal flowing displacement is positively correlated with stress according to the stress distribution in deformation area.

4.3 Microstructure and hardness

The results of the microstructure and hardness of the part were obtained by experiments. The hardening capacity could be calculated by Eq. (4):

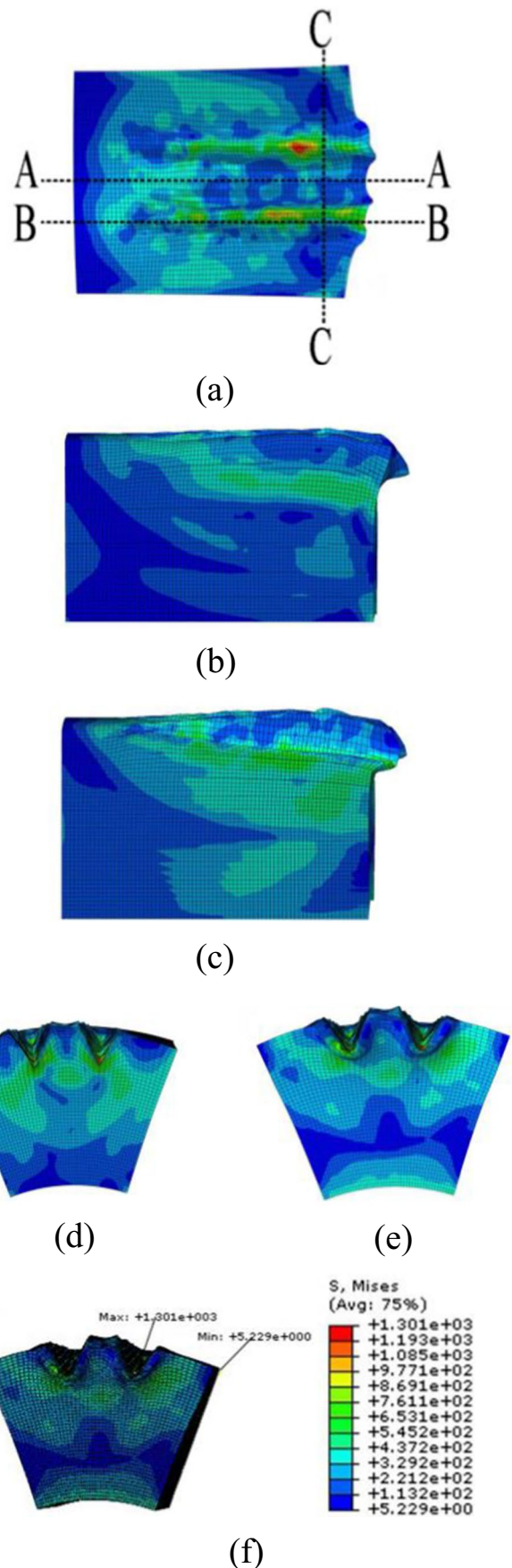
$$N = \frac{Hv - Hv_0}{Hv_0} \times 100\% \tag{4}$$

where Hv is hardness of test points on tooth surface and Hv_0 is hardness of raw material.

The hardening capacity is shown in Table 2.

As shown in Fig. 10, microstructure at top land (area 1) is similar to that at the center of tooth (area 4); there is no fibrous tissue. There is a small amount of fibrous tissue at the location of the tooth side (area 2) and a dense fibrous tissue at the location of the bottom land (area 3). The fibrous tissue on the tooth side and the bottom land is distributed along the tooth shape.

As shown in Fig. 11, the figures of the hardness of tangent of addendum circle, reference circle, and dedendum circle all show the shape of “valley” and have symmetry. The hardness of the top land, tooth side, and bottom land of the tooth



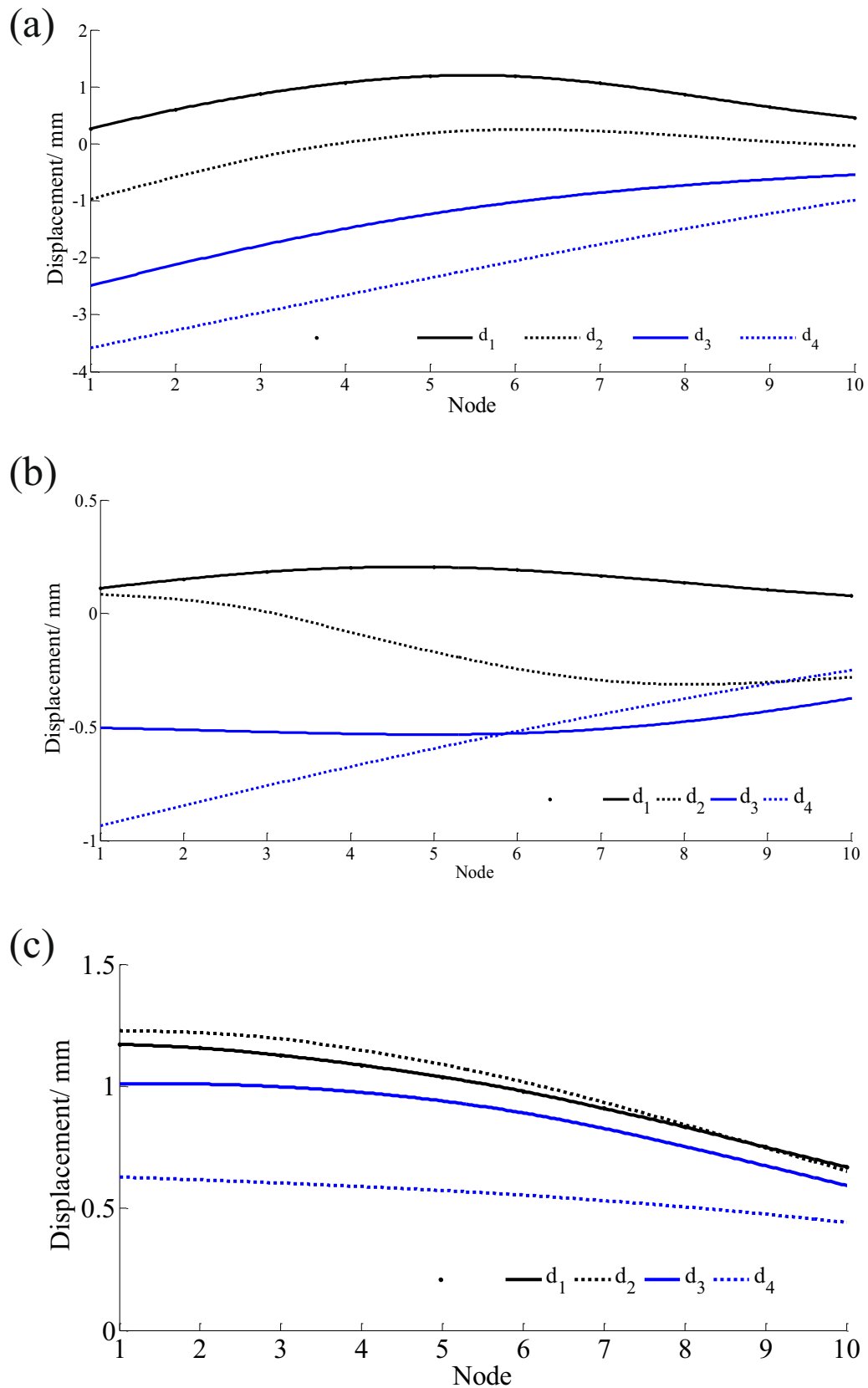


Fig. 5 Radial direction nodal displacement at the **a** x-axis, **b** y-axis, **c** z-axis

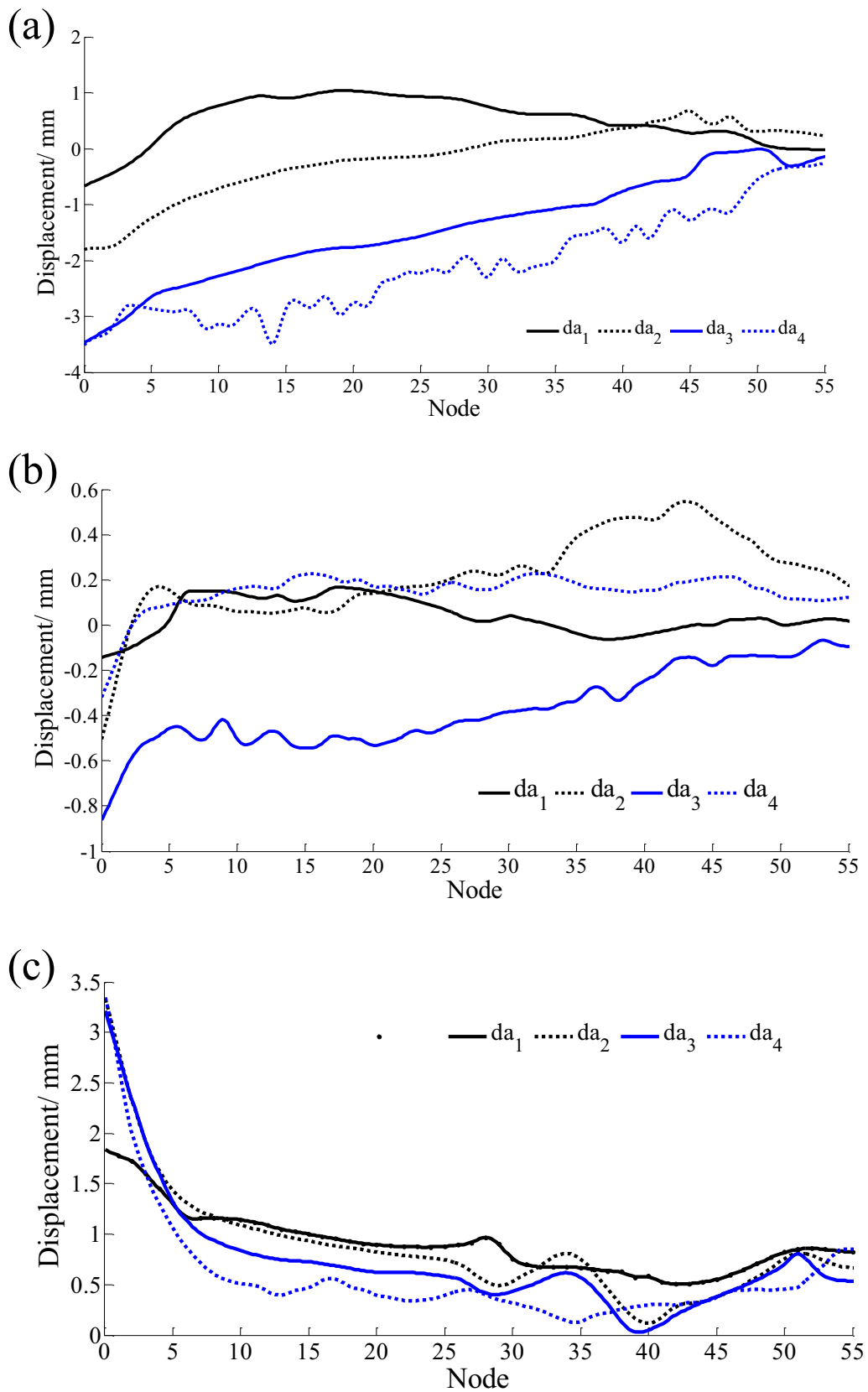


Fig. 6 Nodal displacement of axial direction at the a x-axis, b y-axis, c z-axis

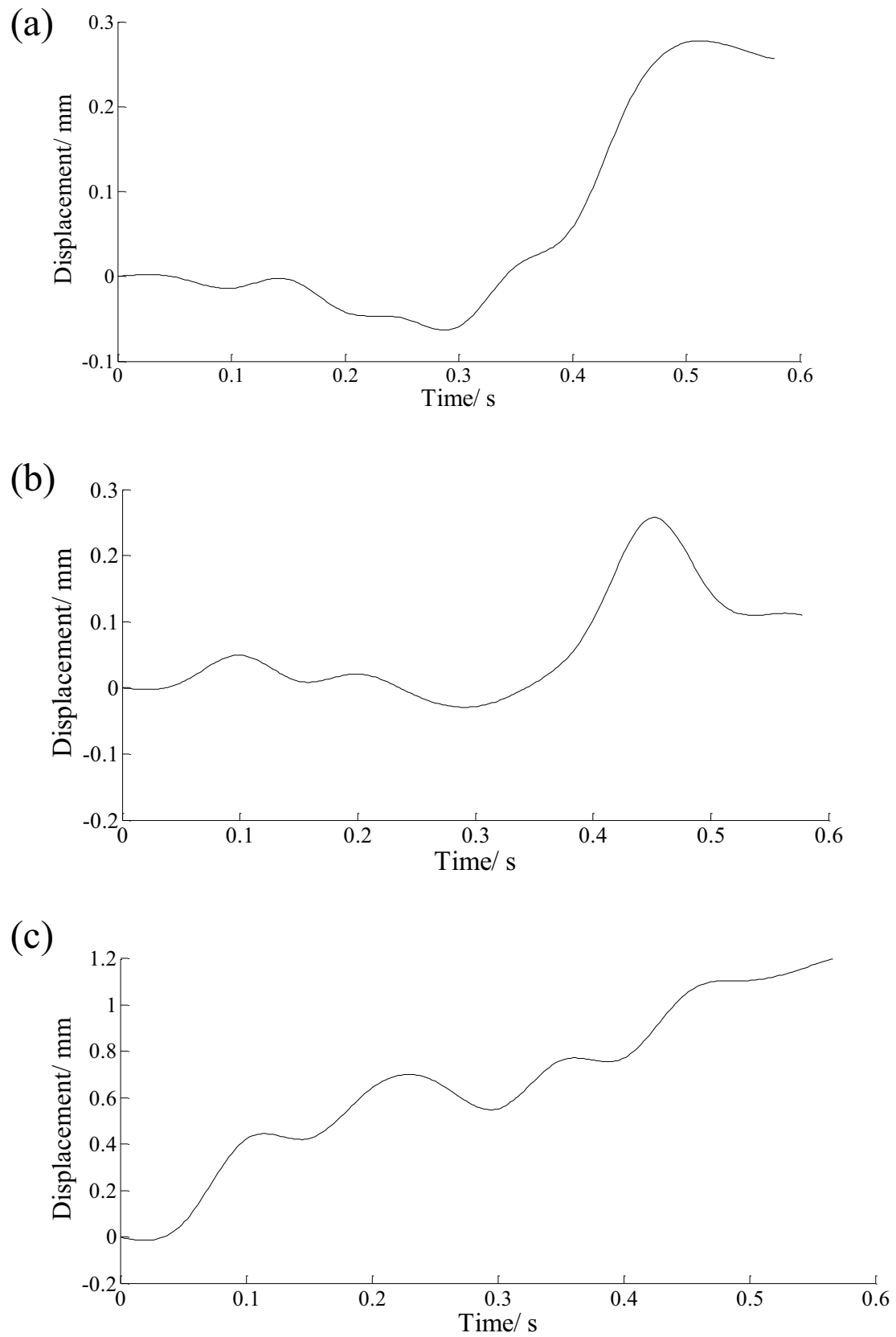


Fig. 7 Addendum nodal displacement (n_1) at the **a** x-axis, **b** y-axis, **c** z-axis

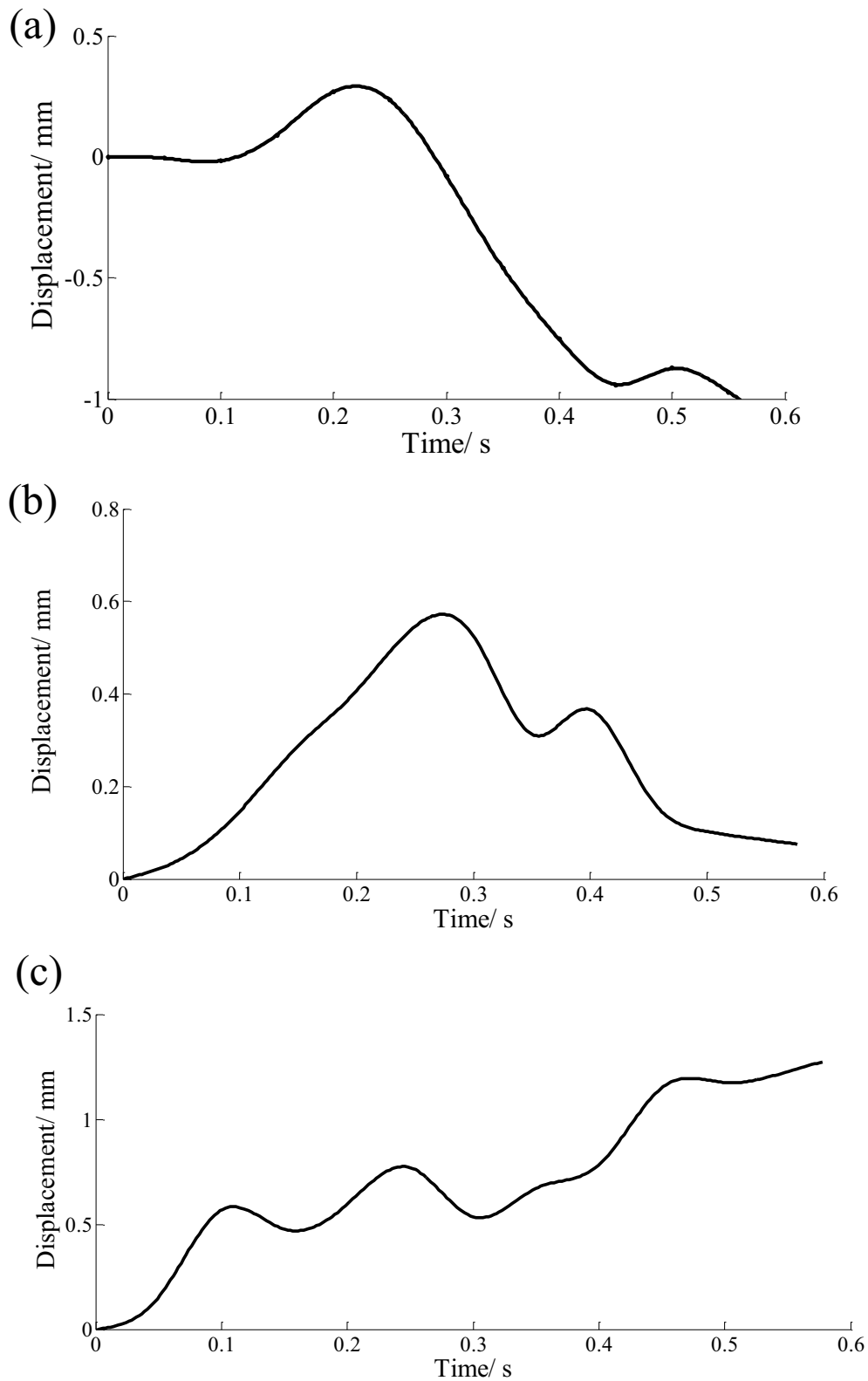


Fig. 8 Nodal displacement of the tooth side (n_2) at the **a** x-axis, **b** y-axis, **c** z-axis

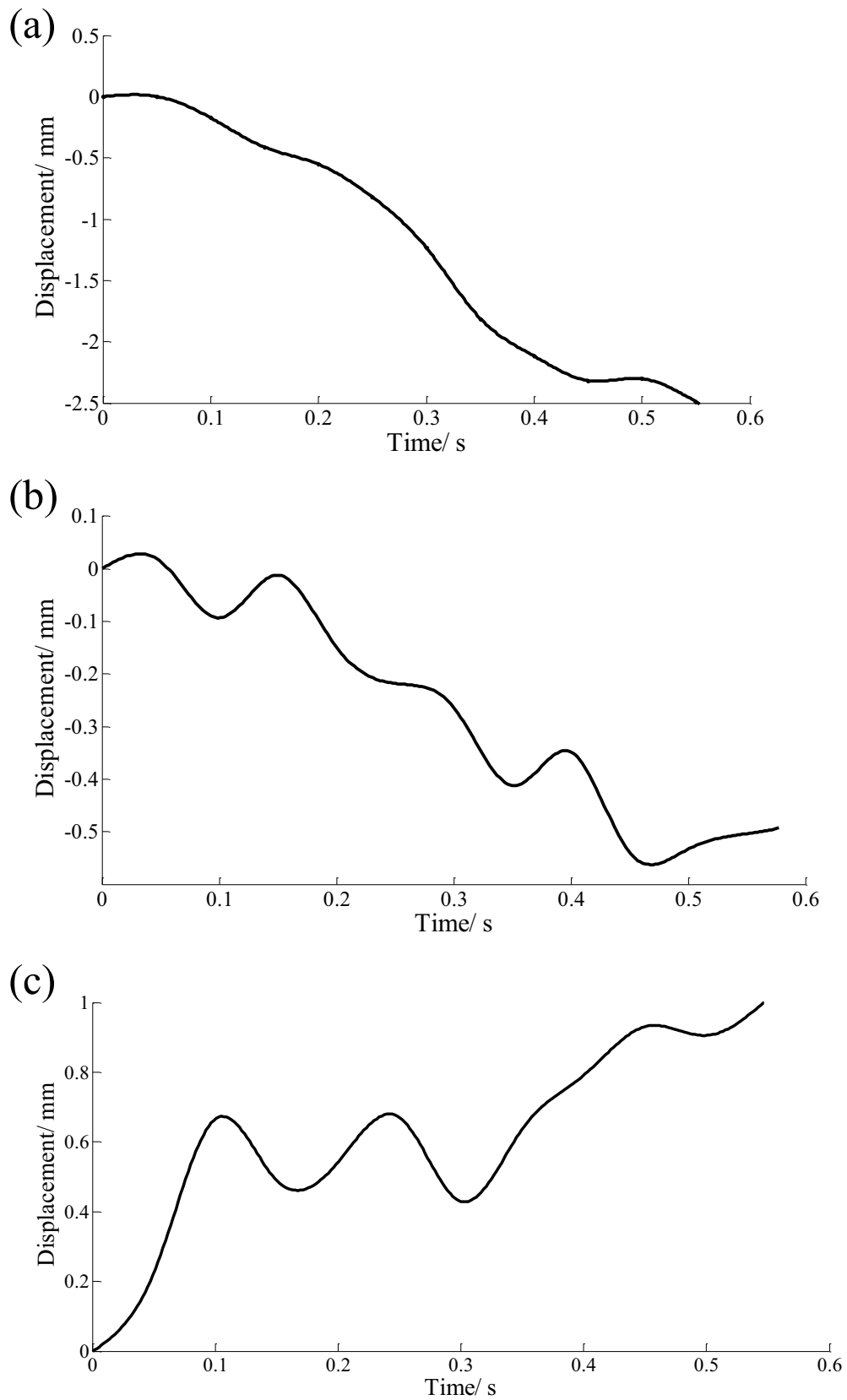


Fig. 9 Dedendum nodal displacement (n_3) at the **a** x-axis, **b** y-axis, **c** z-axis

Table 2 Hardening capacity

Position	Hardening capacity
Top land	18%
Tooth side	22%
Bottom land	28%

increases successively, and the hardness gradually decreases from the surface to the inside of the tooth.

Compared with the FEA forming part in Fig. 2 and test sample in Fig. 3, the contact area forms a tooth groove, and both sides of the groove are raised to form the spline tooth, the top of the tooth is raised, and the end face is protruded. The shape of the FEA tooth is the same as that of the experimental tooth. The metal flowing displacement of FEA is consistent with the metal flowing direction showed by the shape of spline tooth in experiment. Where the degree of microstructure deformation is large, the metal flow displacement is also large. Similarly, the capacity of work hardening is large, and the metal flow displacement is also large. The results of the experiments match the results of the FEA.

5 Discussion

According to the principle of HSCR B, the contact area is groove, that is, the area near the bottom land, where the stress is generated and transmitted from the contact area to the surrounding and gradually decreases. For the cross section of tooth, the stress transmit path is the bottom land, tooth side and top land. The stress of the area where the metal is easy to flow is released. Therefore, the stress decreases successively in the bottom land, tooth side, and top land. In the axial direction, the closer the distance between the groove and the top land, the closer the stress value. Stress drives metal flow.

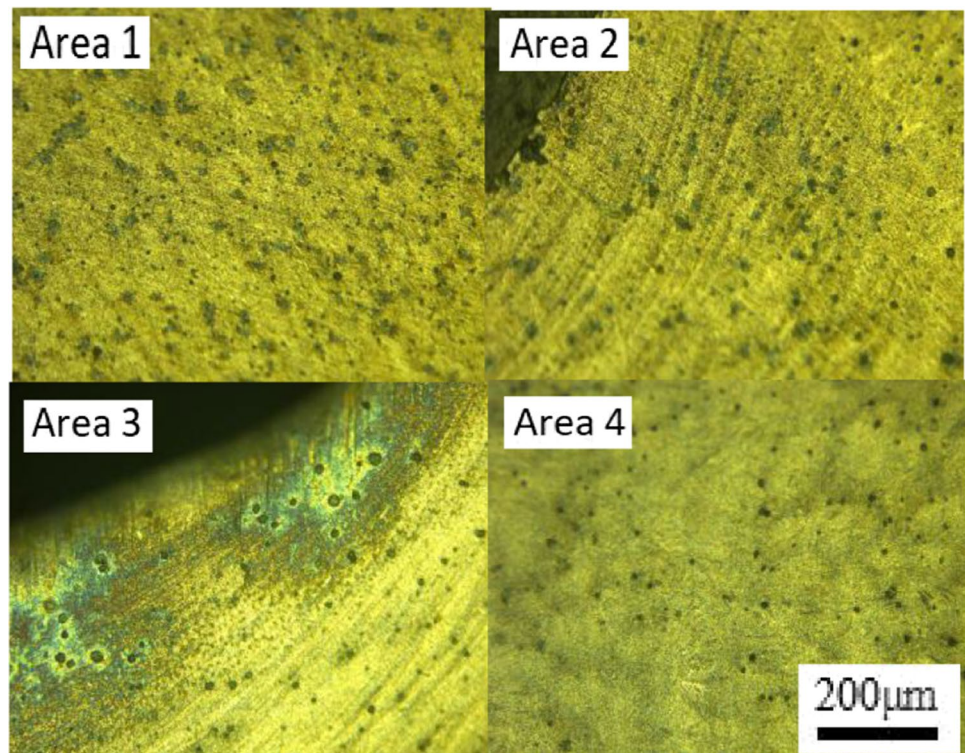
5.1 Metal flow

According to the law of least resistance and the shape of the workpiece, the closer to the workpiece center, the larger the resistance, and the closer to the surface of workpiece, the smaller the resistance.

As shown in Fig. 12a, for the cross section of tooth, the contact area is subjected to the extrusion force from the roller to the center of the workpiece, that is, the force in the *x*-axis direction, so that the metal flows to the center of the workpiece.

As shown in Fig. 12c, for the area which is near the bottom land, the shape of the roller causes the normal

Fig. 10 Microstructure of HSCR B



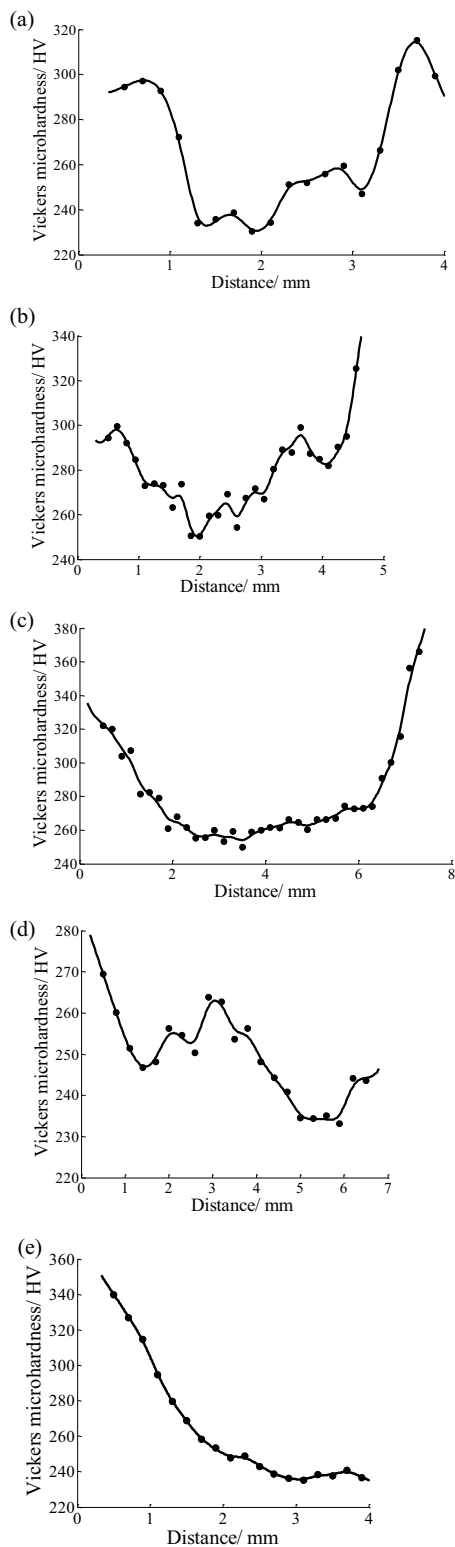


Fig. 11 Hardness of the tooth surface. **a** Tangent of addendum circle (l_1). **b** Tangent of reference circle (l_2). **c** Tangent of dedendum circle (l_3). **d** Center line of the top land (l_4). **e** Center line of the groove (l_5)

component of the force F_{ny} . Therefore, the metal flows in the normal direction, that is, the metal flows to both sides of the roller, and the metal extrudes the surrounding metal. For the tangential force component F_{ty} , due to the constraint in the direction of the y -axis, the metal is difficult to flow in the direction; therefore, the metal flows in the direction of the x -axis.

As shown in Fig. 12d, the position of the tooth side is mainly effected by the groove. The force decomposition shows that the metal flows towards the direction of the groove due to the force in the positive direction of y -axis and the negative direction of x -axis.

As shown in Fig. 12e and Fig. 13, the metal of top land flows to the direction of the groove due to the affection of the groove. The position is also effected by the metal which is extruded on both sides of the roller. Therefore, the metal flows in the direction of least resistance, that is, the position of the workpiece surface. The metal flows in the positive direction of x -axis and the positive direction of y -axis.

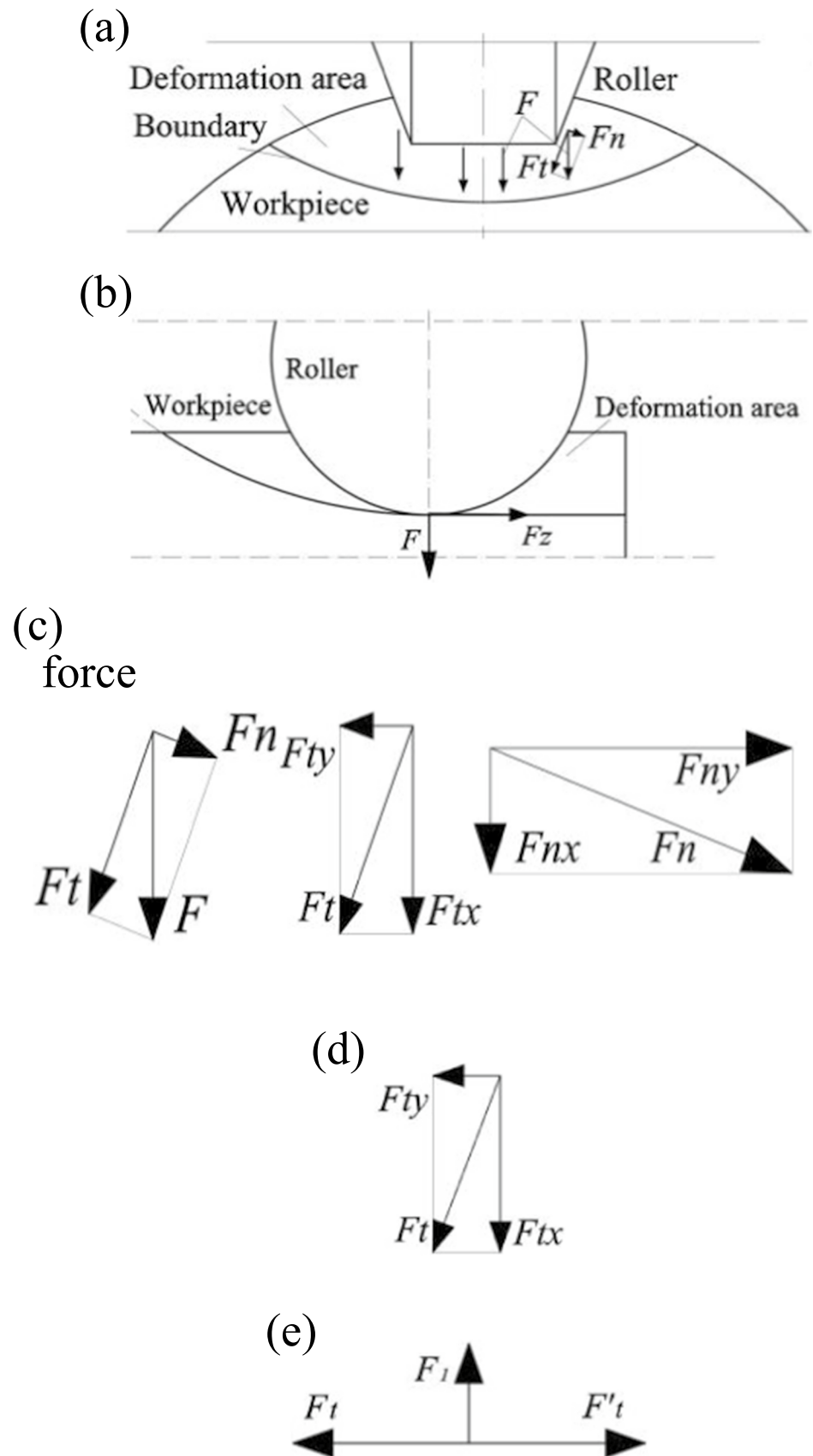
As shown in Fig. 12b, in the z -axis direction, no matter where the displacement is affected by the roller, the direction of effection is the component of the roller in the positive direction of z -axis; therefore, the movement direction of the roller determines the flow direction of the metal.

In short, the metal of the groove is forced to flow due to the groove occupied by the roller, and the surrounding metal is extruded to flow in the direction of least resistance, which is the workpiece surface. Therefore, the surface protrudes to the direction of the top of the tooth, while in the direction of z -axis, the end face also protrudes. The involute spline tooth is obtained by the forming due to the shape of the roller; therefore, roller plays a decisive role in metal flow. Combined with stress and metal flow, it can be seen that in the deformation area, the greater the stress, the greater the metal flowing displacement, and the more severe the plastic deformation. And the closer to the contact position, the greater the stress.

5.2 Microstructure

As shown in Fig. 14, the force of bottom land is decomposed into the normal force F_n and the tangential force F_t . It is decomposed into normal force F'_n and tangential force F'_t by the reaction force from the workpiece material. The microstructure is compressed by the normal force and is elongated by the tangential force. The direction of tangential force and normal force is closely related to the shape of the roller; therefore, the microstructure deformed along the direction of deformation, which determines the distribution of the fibrous tissue along the tooth shape.

Fig. 12 The force analysis of HSCRB. The force of **a** cross section, **c** bottom land, **d** tooth side, **e** top land. **b** Axial force



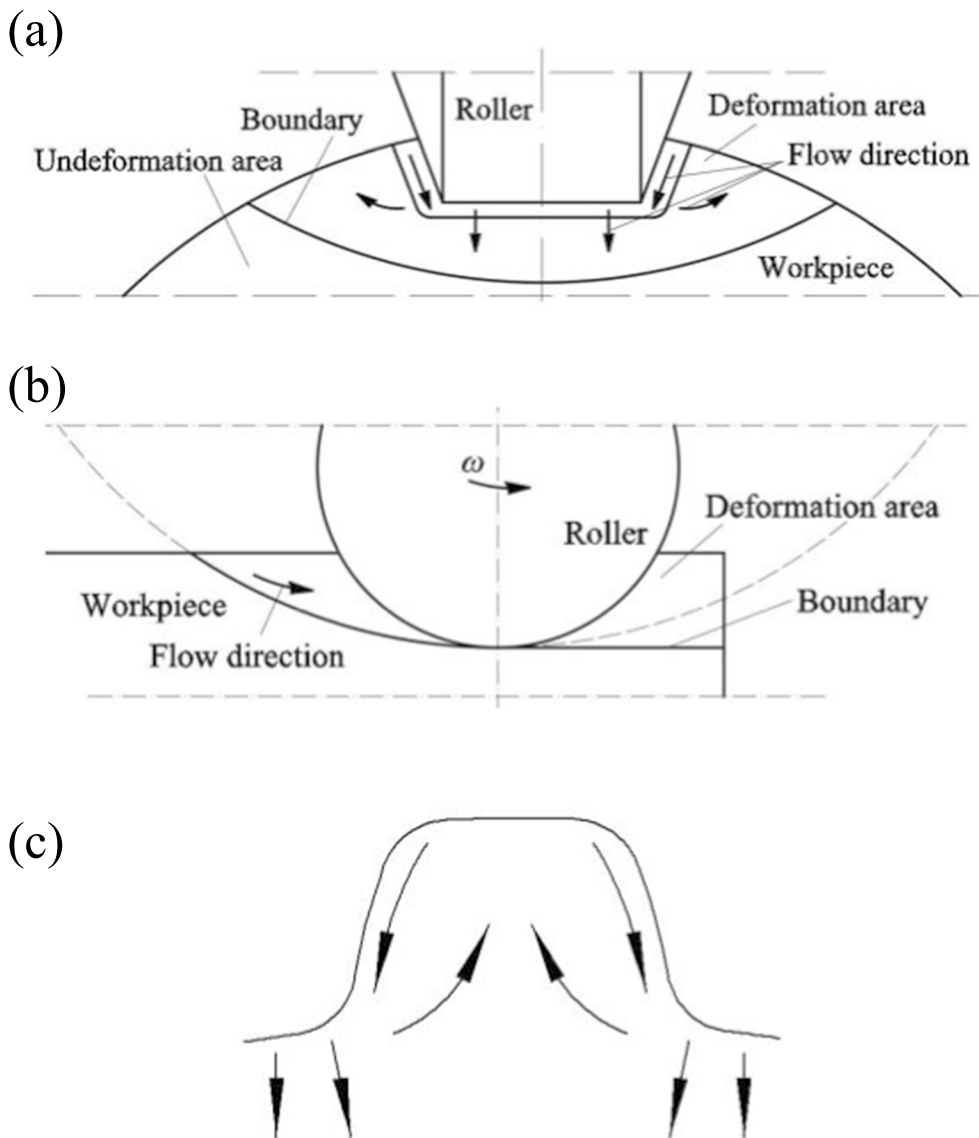
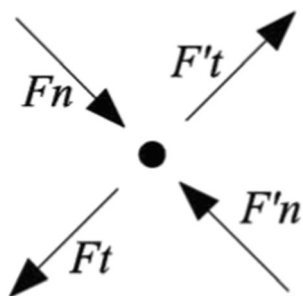


Fig. 13 Metal flow of HSCRB at the a cross section of workpiece, b z-axis of workpiece, c cross section of tooth

Fig. 14 Formation of fibrous tissue



The larger the flow displacement, the longer the grains are pulled. The flow displacement at the bottom land is sufficient to elongate the grains and form fibrous tissue. For other positions, the displacement determines that little or no fibrous tissue could be formed. With the distance increasing from the deformation area, the effect of deformation decreases until the original state. Therefore, the flow displacement determines the change degree of the microstructure, and there is a positive correlation.

5.3 Work hardening

The work hardening is related to the characteristics of microstructure, the flow produces fibrous tissue, and the fibrous tissue obtained by cold forming increases the deformation resistance of the parts, and the hardness and strength are significantly increased, and the mechanical properties of the parts are strengthened.

According to the characteristics of the cold forming fibrous tissue [19], the density of the fibrous tissue is positively correlated with the degree of work hardening. Dense fibrous tissue is distributed in the bottom land, and the degree of hardening is the highest. There is a small amount of fibrous tissue on the tooth side, and its hardness is less than that of the bottom land.

Although there is no fibrous tissue at the top land, the hardening effect is produced by the metal flow, and the hardness is less than that of the tooth side and bottom land. With the increase of the distance from the deformation area, the hardness gradually decreases to the original hardness of the material, which is characterized by high surface hardness but great core toughness.

In addition, according to the principle of plastic forming, the greater the degree of deformation, the greater the capacity of work hardening. Therefore, from the perspective of metal flow displacement, the greater the flow displacement, the greater the hardness, which explains that the bottom land, tooth side, and top land hardness gradually decreased, and the hardness gradually decreased from tooth surface to interior.

The shape and mechanical properties of parts changed during forming at the same time. The surface and microstructure of the parts are intact no damaged. Avoiding the machining damage microstructure, which led to the decrease of the mechanical properties. Because of work hardening and to strengthen the mechanical properties of the change of microstructure, the mechanical properties meet the requirement of tooth shape of parts. In addition, the process parameters and the shape of the roller could be used to control the metal flow to achieve the control and improvement of the forming quality.

6 Conclusion

Through analysis of stress distribution, metal flow, microstructure, and work hardening, the metal flow mechanism of involute spline high-speed cold roll beating was studied, and the following conclusions were drawn:

- (1) The stress distribution of the parts is as follows: the groove and bottom land are the largest, and the tooth side and top land decrease in turn. The stress is trans-

mitted outwards from the deformation area and gradually decreases with the increase of the distance.

- (2) The characteristics of metal flow are that the metal in the groove flows to the inner of the workpiece and extrudes the surrounding metal to flow to the surface of the workpiece with least resistance. The metal of tooth side and top land flows along the tooth shape to the direction of the groove. The farther away the area from the groove, the less effected by the forming, and the smaller the flow. And the teeth would be affected by the forming of the adjacent groove. The flow displacement of the bottom land, tooth side, and top land decreases successively, while the other positions are negatively correlated with the distance of the contact position.
- (3) The relationships between metal flow and microstructure and mechanical properties of parts were explored. The change of microstructure caused by metal flow and the flow displacement determine the amount of fibrous tissue, which is manifested in large number of fibrous tissue at the bottom land, a small amount of fibrous tissue at the tooth side, and little fibrous tissue at the top land. The work hardening capacity is related to the distribution of the fibrous tissue of the part and metal flow.
- (4) By studying the metal flowing mechanism of high-speed cold roll beating, the forming characteristics of the process and the property characteristics of the forming parts were obtained, which lay a foundation for further research on quality control during forming.

Funding The research is supported by the National Natural Science Foundation of China (Grant No. 51275331); Shanxi Provincial Key Research and Development Project (Grant No. 201903D121041), China; and the Support Plan for Outstanding Youth Academic Leaders in Colleges and Universities of Shanxi Province, China.

Availability of data and material The data and material are within in the manuscript.

Code availability Not applicable.

Declarations

Ethics approval Not applicable.

Consent to participate Not applicable.

Consent for publication Not applicable.

Conflict of interest The authors declare no competing interests.

References

- Li YT, Ju L, Niu T, Song JL, Liu ZQ (2015) Research status and development trend on cold forming of tooth-like shaft parts. *Journal of Taiyuan University of Science and Technology* 35(3):165–169
- Krapfenbauer H (1994) New methods to cold roll splines on hollow blanks. *European Production Engineering* 1(9):39–43
- Cui FK, Su YX, Xie KG, Ding ZH, Li YX, Li Y, Li CM (2018) Research on distribution law of residual stress in surface layer of cold roll-beating spline. *Acta Armamentarii* 39(05):1022–1032
- Li L, Li Y, Yang MS, Xiao XD, Cui LM, Cui FK (2019) Effects of process parameters on forming force and accuracy in cold roll-beating forming external tooth groove. *Int J Adv Manuf Technol* 100:2229–2242. <https://doi.org/10.1007/s00170-018-2844-6>
- Niu T, Li YT, Wang LM, Lu HY (2017) Analysis on forming effect between adjacent cogging of cold strike spline. *Forging & Stamping Technology* 42(11):66–72
- Tian SQ, Du SW, Li YT, Niu T (2017) Modal analysis on spline shaft of cold-striking machine based on ANSYS Workbench. *Forging & Stamping Technology* 42(11):109–114
- Ma ZY, Luo YX, Wang YQ, Willens DC (2019) Numerical and experimental investigation on material flow in gear forced throughfeed rolling process. *Int J Adv Manuf Technol* 104:3361–3381. <https://doi.org/10.1007/s00170-019-03895-9>
- Deng L, Dai WL, Wang XY, Jin JS, Li JJ (2018) Metal flow controlled by back pressure in the forming process of rib-web parts. *Int J Adv Manuf Technol* 97:1663–1672. <https://doi.org/10.1007/s00170-018-1883-3>
- Wang YP, Li F, Shi WY, Li XW, Fang WB (2019) Dynamic recrystallization and metal flow behavior of AZ31 magnesium alloy bending products processed by staggered extrusion. *J Mater Eng Perform* 28(6):3551–3559. <https://doi.org/10.1007/s11665-019-04133-9>
- Shen XH, Chen W, Yan J, Zhang L, Zhang J (2015) Experiment and simulation of metal flow in multi-stage forming process of railway wheel. *J Iron Steel Res Int* 22(1):21–29. [https://doi.org/10.1016/s1006-706x\(15\)60004-8](https://doi.org/10.1016/s1006-706x(15)60004-8)
- Wang ZH, Zhan WT, Hong XX, Bao GJ, Yang QH (2017) Characteristics of metal flow in cold extrusion under electric-hydraulic chattering. *J Iron Steel Res Int* 24(2):138–146. [https://doi.org/10.1016/s1006-706x\(17\)30020-1](https://doi.org/10.1016/s1006-706x(17)30020-1)
- Svirin VV, Solomonov KN (2010) Effect of friction on the kinematics of metal flow. *Metallurgis* 54(5–6):362–366. <https://doi.org/10.1007/s11015-010-9304-3>
- Yi J, Wang ZH, Liu ZW, Zhang JM, He X (2018) FE analysis of extrusion defect and optimization of metal flow in porthole die for complex hollow aluminium profile. *Transactions of Nonferrous Metals Society of China* 28(10):2094–2101. [https://doi.org/10.1016/s1003-6326\(18\)64853-8](https://doi.org/10.1016/s1003-6326(18)64853-8)
- Zhao JW, Wang XC, Yang Q, Wang QN, Wang YY, Li WP (2021) Mechanism of lateral metal flow on residual stress distribution during hot strip rolling. *Journal of Materials Processing Tech* 228:116838. <https://doi.org/10.1007/s00170-016-8973-x>
- Löffler M, Schulte R, Freiburg D, Biermann D, Stangier D, Tillmann W, Merklein M (2019) Control of the material flow in sheet-bulk metal forming using modifications of the tool surface. *Int J Mater Form* 12:17–26. <https://doi.org/10.1007/s12289-018-1399-2>
- Pilz F, Merklein M (2020) Influence of component design on extrusion processes in sheet-bulk metal forming. *Int J Mater Form* 13:981–992. <https://doi.org/10.1007/s12289-019-01522-2>
- Tumbajoy-Spinel D, Maeder X, Guillonneau G, Sao-Joao S, Descartes S, Bergheau JM, Langlade C, Michler J, Kermouche G (2018) Microstructural and micromechanical investigations of surface strengthening mechanisms induced by repeated impacts on pure iron. *Mater Des* 147:56–64
- Grassino J, Vedani M, Vimercati G, Zanella G (2012) Effects of skin pass rolling parameters on mechanical properties of steels. *Int J Precis Eng Manuf* 13(11):2017–2026
- Liu ZQ, Song JL, Li YT, Li XD (2011) Analysis and experimental study on the precision cold rolling process of involute spline. *Journal of Mechanical Engineering* 47(14):32–38
- Wang P, Yin T, Qu S (2020) On the grain size dependent working hardening behaviors of severe plastic deformation processed metals. *Scripta Mater* 178:171–175
- Rule WK, Jones SE (1998) A revised form for the Johnson-Cook strength model. *Int J Impact Eng* 21(8):609–624
- Xu ZJ, Liu Y, Hu HZ, He XD, Huang FL (2019) Determination of shear behavior and constitutive modeling of the 603 steel over wide temperature and strain rate ranges. *J Mech Phys Solids* 129(8):184–204
- Chen G, Chen ZF, Tao JL, Niu W, ZHANG QP, Huang XC (2005) Investigation and validation on plastic constitutive parameters of 45 steel. *Explosion and Shock Waves* 25(5):451–456

Publisher's Note Springer Nature remains neutral with regard to jurisdictional claims in published maps and institutional affiliations.